PROCEEDINGS OF SCIENCE

Large area hybrid detectors at Sirius: Operation threshold optimization for Medipix3RX

Matheus G. Fernandes,* **Raul B. Campanelli, Gustavo S. Gomes, Erick B. Antonio and Jean M. Polli**

Brazilian Synchrotron Light Laboratory,
13083-100, Campinas, Brazil

E-mail: matheus.fernandes@lnls.br

At the Sirius synchrotron facility, large area photon counting detector systems are employed in different beamlines and experimental techniques. These detectors were developed at the Brazilian Synchrotron Light Laboratory (LNLS), the called PIMEGA series detectors feature Medipix3RX Application Specific Integrated Circuit (ASIC), with 256 x 256 squared pixels and 55 µm pitch. In this work, the influence of the threshold energy level was evaluated in order to achieve optimized values for minimizing false counts during operation, which arise from the charge sharing effect. As a result, we have defined the Approximated Mean Multiplicity (AMM), which can be used as a new procedure in photon counting detectors to define an optimal operation threshold level. Additionally, energy calibrations and energy resolution experiments are presented, as well as the AMM values for multiple operation bias voltages and incident energies.

Pixel 2022 - 10th International Workshop on Semiconductor Pixel Detectors for Particles and Imaging,
12-16 December 2022
La Fonda Hotel, Santa Fe, New Mexico, USA

*Speaker

PoS(Pixel2022)066

1. Introduction

Hybrid detectors are widely used for large area radiation imaging at synchrotron facilities. Among the reasons that make this kind of device appealing are the low noise level, energy discrimination, and relatively high count-rate capabilities, as recently described by our group on the PIMEGA detectors [1].

These detectors operate with a threshold level that will allow the circuit to count photons, whose energy produces current pulses greater than the threshold level setting. In this work, the influence of this threshold level was evaluated to achieve optimized values to mitigate false counts originating from the charge sharing effect. Additionally, energy calibrations and energy resolution experiments are presented.

1.1 Sirius detectors systems

Developed and present in beamlines at Sirius Synchrotron, the PIMEGA series of hybrid pixels detectors feature Medipix3RX [2] Application Specific Integrated Circuit (ASIC), with 256 x 256 squared pixels and 55 µm pitch. The PIMEGA series comprehends detectors of different area, geometry and sensors. These detectors can feature sensors of Si 300 or 675 µm and CdTe 1mm thick, and are able to achieve framerates up to 2000fps for detectors with 9.4 MP of active area. A picture of PIMEGA 135D is depicted in Figure 1.

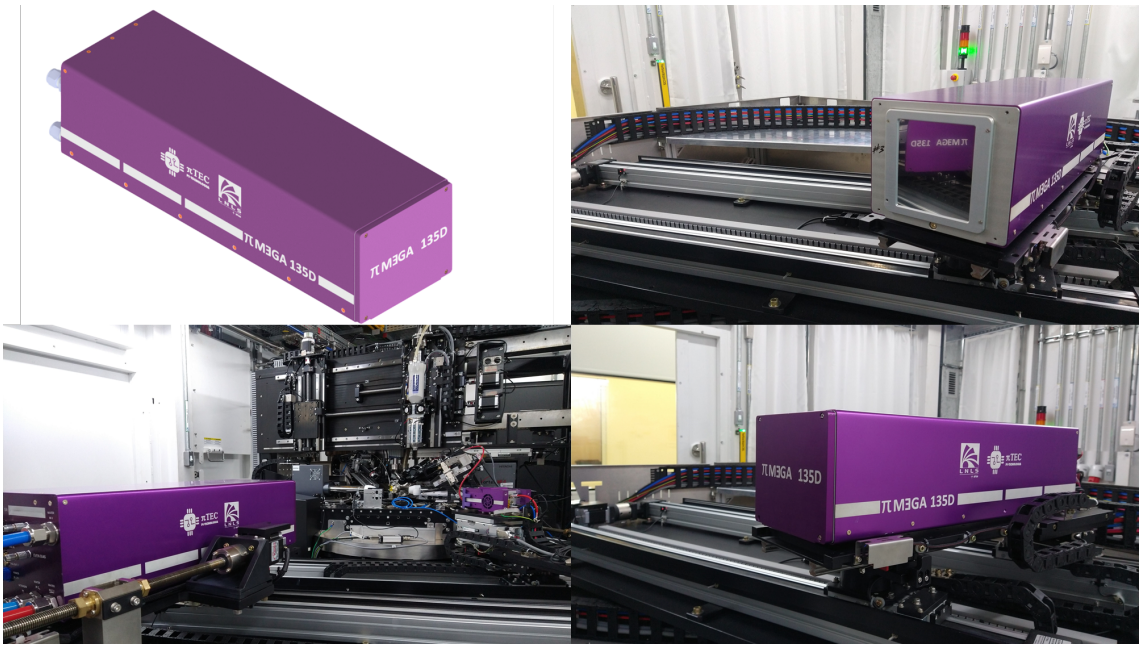

Figure 1: Pimega 135D 3D render and pictures at *Carnaúba* beamline [3].

1.2 The 50% incident energy threshold procedure

Photon counting detectors featuring energy threshold level usually are operated by choosing this level value as half of the incident energy [4]. This choice is made in order to filter the electronic noise, as well as eliminate part of the charge sharing effect.

This procedure [4] was evaluated only for energies of 13 keV and higher, and for these cases, the model shows three or more pixels events are negligible, so the events are analyzed as if only two pixels can share the charge. Thus the conclusion of the authors in [4] is that a 50% of incident energy threshold will mitigate the charge sharing effect, since this way only one of these two pixels will be able to count a single photon.

However the physical causes of the charge sharing effect are still present, the electronic systems will just not be able to notice this effect when working with a higher optimal threshold level. The causes for the charge sharing effect can be pointed out: the charge carrier diffusion cloud reaching the pixels, the electric field drift, as well collisions with doping points, impurities, and non-uniformities. It's interesting to point out that during the digital-analog converter (DAC) threshold calibration towards the energy the detector is already suffering from the charge sharing effect. So even with this procedure the charge sharing effect still has an influence over the detector.

In this work lower energies were evaluated, which showed a different behavior of the charge sharing effect where the threshold of half of the incident energy was not sufficient to mitigate the charge sharing procedure.

1.3 The Charge Summing Mode

The Charge Summing Mode (CSM) is a mode of operation created to reduce the charge sharing effect, while it also brings better spatial resolution and reduced low energy tail [5]. The idea of this operating mode is to work with clusters of 2x2 pixels that, the pixels, can communicate with each other in order to check if a charge originating from the same photon is only counted once.

When not operating in CSM, where the pixels count their own pulses without any kind of communication between them, we call it Single Pixel Mode (SPM).

When working with a noise equalization method, in the CSM TS the fluorescence peaks will appear in a position before the SPM TS, while the x-axis is in DAC step threshold unit. This occurs because the electronic noise in CSM mode is higher than SPM, making the target threshold associated with the noise cause a shift in the DAC threshold axis.

However, SPM is the traditional mode of operation of X-ray detectors, because although CSM has its before-mentioned advantages, its energy resolution is worse than SPM [5]. Therefore each mode of operation has its unique advantages for different applications: using CSM for better spatial resolution and using SPM for better energy resolution.

2. Experimental methods

In this characterization work a co-planar geometry detector (all sensors in the same plane of detection) of 1536x1536 active pixels (about 2.36 MP) with 300µm thick Si sensors was studied. The experiments used High Gain Mode (HGM), 12 bits dynamic range (up to 4095 counts per pixel) and 2s of acquire time.

All experiments were conducted in standard ambient temperature and pressure (SATP) conditions. The detector was equalized using a noise-based equalization [6]. A fluorescence setup was employed, using a portable x-ray tube (Amptek Mini-X2), operating in 50kV/200µA, encased in a lead insulated box pointing to a fluorescence target, which was variable between Mn ($K\alpha_1$ = 5.898keV), Ni ($K\alpha_1$ = 7.478keV) and Cu ($K\alpha_1$ = 8.047keV). The fluorescence is able to reach the

detector through a hole in the box pointing to the detector. The box was placed 15cm from the detector, with the hole centralized with its sensors.

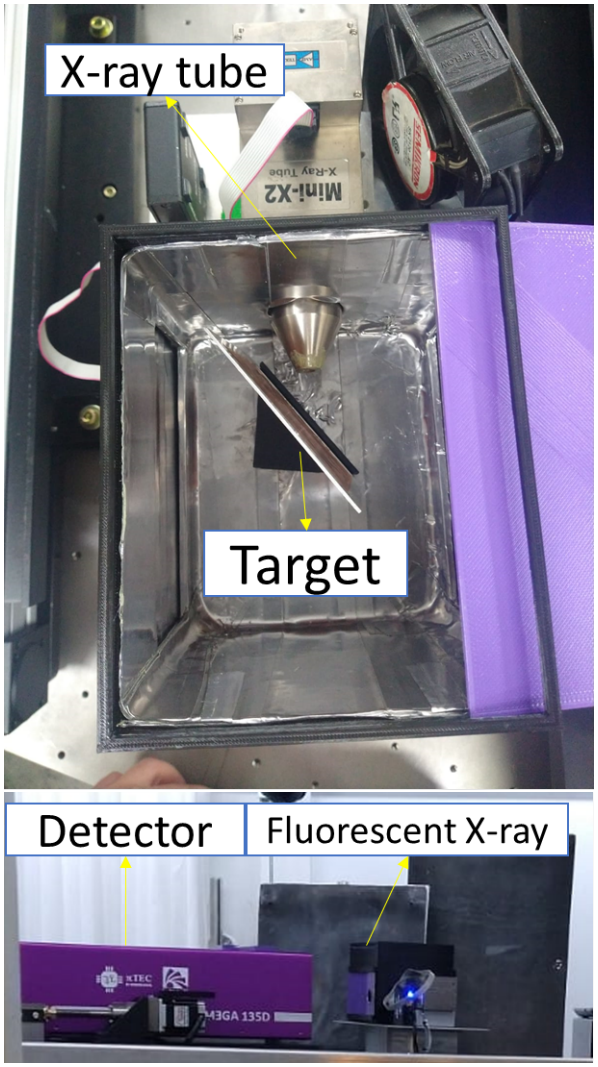

Figure 2: Top view of the lead insulated box and the setup pointing to the Pimega 135D at *Carnaúba* beamline [3].

Threshold scans were performed in different fluorescence targets, bias voltage and operation mode (SPM and CSM). A flatfield-based correction (generated with 9.8keV fluorescent photons) was applied to the images used to generate these scans.

3. Results and Discussions

3.1 Energy calibration

The energy calibration is a relation between the threshold represented by DAC steps and the energy values. This relation is often linear, but will suffer effects of the bias voltage, operation mode (SPM or CSM), gain mode, equalization, ASIC, sensor material, and thickness. In this study,

energy calibrations were obtained for different bias voltages and operation modes, while the other variables were fixed. In order to obtain the calibrations, threshold scans were performed for a bias voltage range of 35 to 100V, with step of 5V, for SPM and CSM, using the three available fluorescence targets for a total of 28 calibration curves.

To find the adequate peak position, a differential plot of each threshold scan was constructed and a gaussian fit is executed as shown in Figure 3. With the peak position of the three available targets, we were able to obtain the energy calibration curve, as exemplified in Figure 4 and shown in Figures 5 and 6.

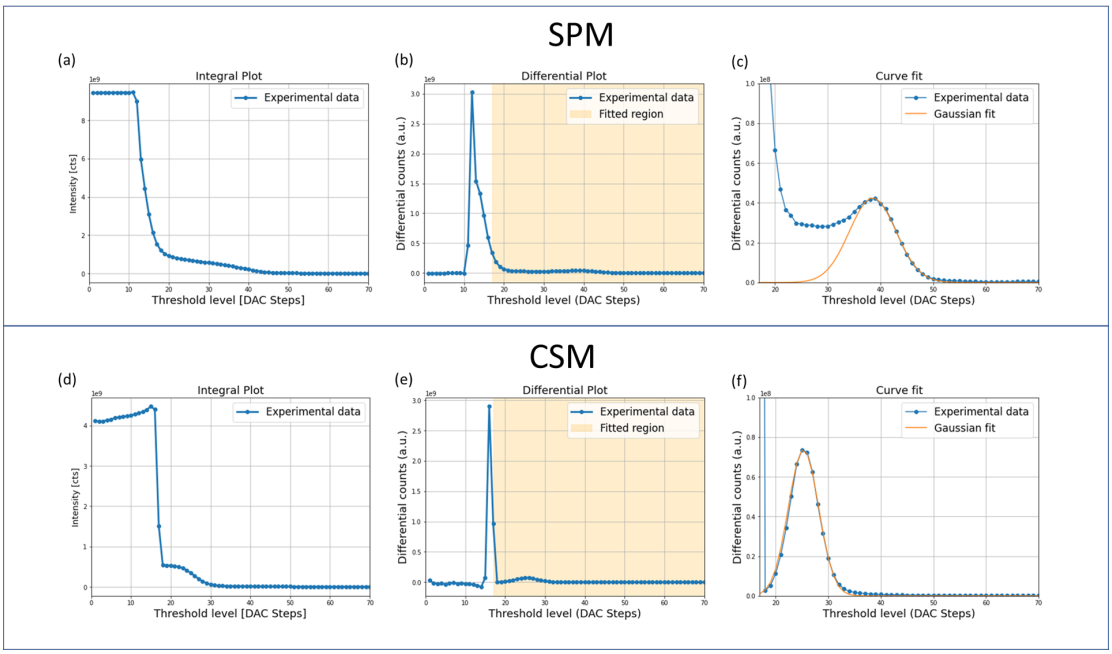

Figure 3: SPM and CSM threshold scans: (a) and (d) integral curves, (b) and (e) differential curves, and (c) and (f) gaussian fitting in a zoom of the highlighted region of the differential curves.

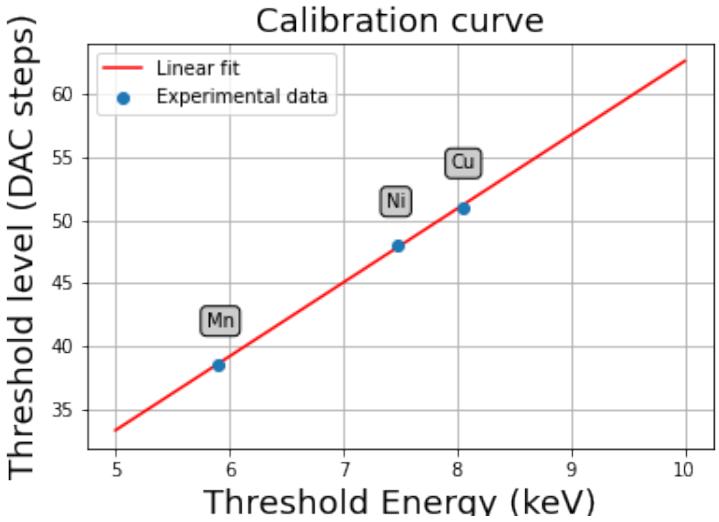

Figure 4: One of the calibration curves - SPM, Bias Voltage = 100V.

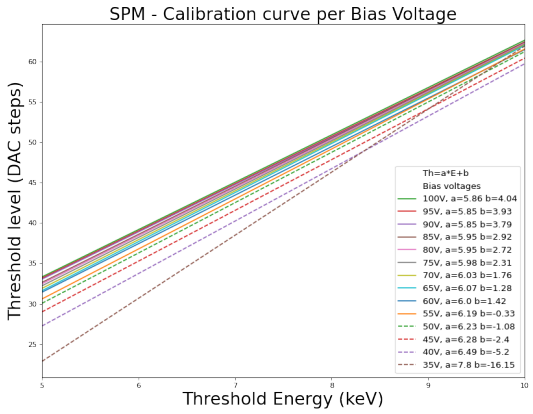

Figure 5: Calibration curves obtained for SPM.

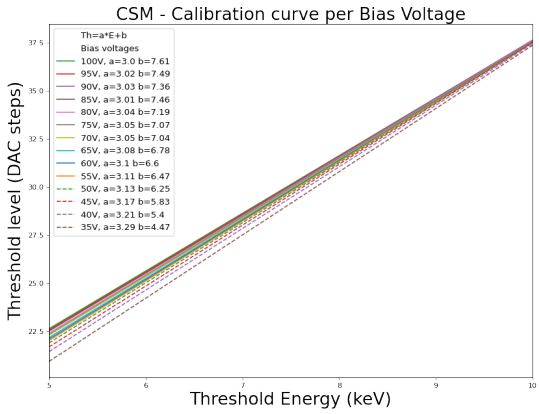

Figure 6: Calibration curves obtained for CSM.

The peak position along the threshold level axis varies depending upon the bias voltage and operation mode, as shown in Figure 7.

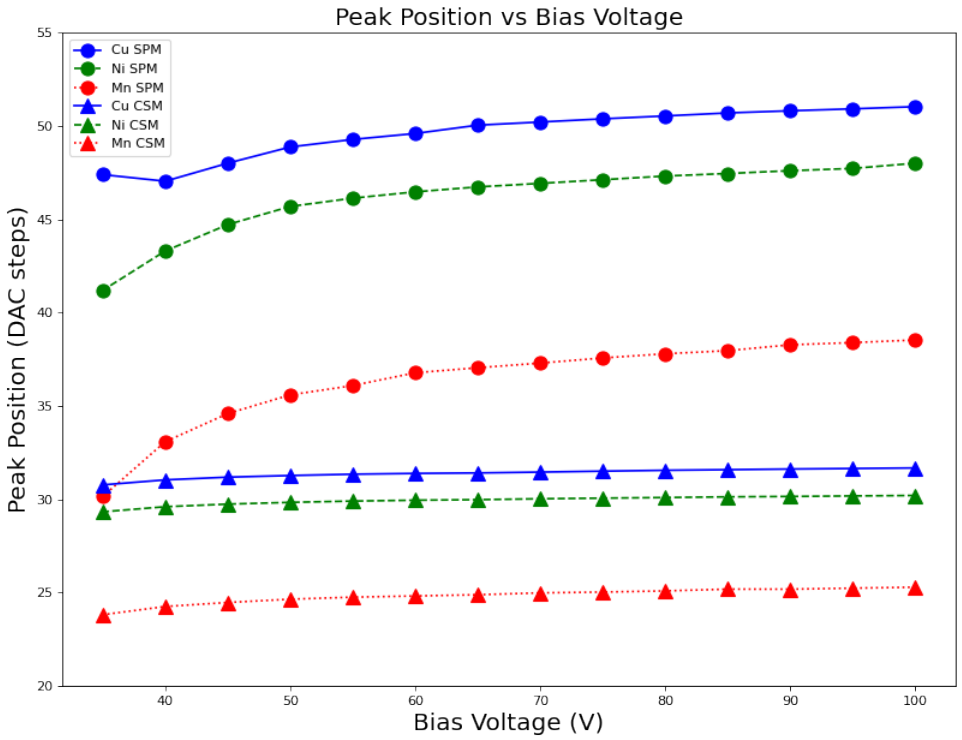

Figure 7: Peak position in DAC steps evaluated in different bias voltages and operation modes.

The following Figure 8, shows the full width at half maximum (FWHM), inversely proportional to the energy resolution for each bias voltage and operation mode. As expected [5] CSM has larger FWHM values (worse energy resolution).

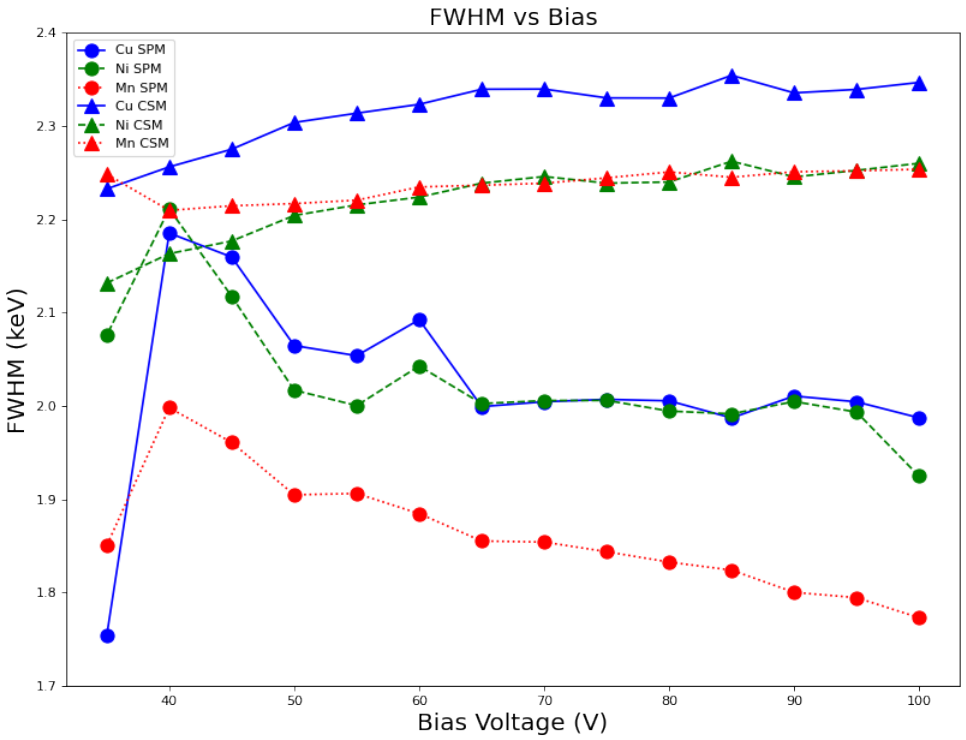

Figure 8: FWHM in different bias voltage and operation modes. The lower the FWHM better will be the energy resolution. An outlier can be seen in the 35V bias, which can be explained by the sensor not being fully depleted.

3.2 Multiplicity and AMM

In order to create a new strategy to choose an ideal value of energy threshold different from the common approach of setting it to half the incident energy, we made an assumption that the CSM corresponds to a mean multiplicity [7] <m>= 1. Therefore we defined the Approximated Mean Multiplicity (AMM), as follows:

$$AMM\left(\frac{SPM_{Counts}}{CSM_{Counts}}\right) = \begin{cases} \frac{SPM_{Counts}}{CSM_{Counts}}, & \frac{SPM_{Counts}}{CSM_{Counts}} \geq 1 \\ 1, & \frac{SPM_{Counts}}{CSM_{Counts}} < 1 \end{cases}$$

The idea is that, since we are considering <m>= 1 for CSM, the $\frac{SPM_{Counts}}{CSM_{Counts}}$ will bring the mean multiplicity value of the SPM TS along the threshold axis. However, simply dividing both curves yields some values under 1 when the threshold starts to filter even the signal, and since there is no physical meaning in counting a photon between 0 and 1 times we defined for those cases the AMM will be equal to 1. By this procedure, an optimal threshold can be defined by the first point

the AMM reaches the value 1 after the noise region. A comparison between $\frac{SPM_{Counts}}{CSM_{Counts}}$, AMM, the selected energy threshold via 50% of the incident energy and the new optimal energy threshold via AMM is presented on Figure 9.

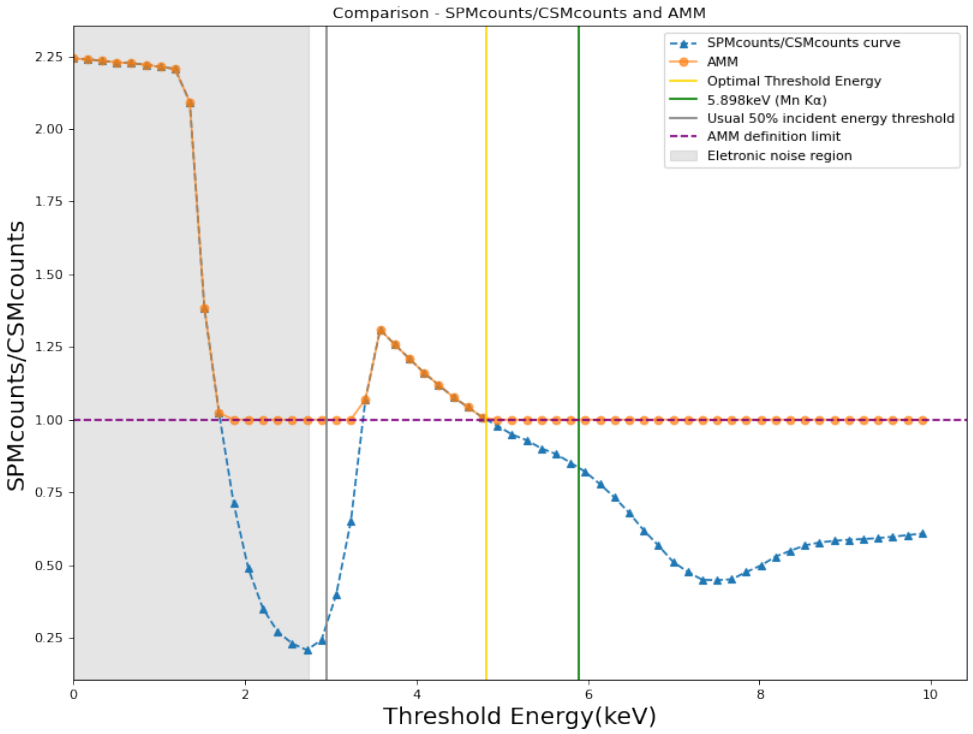

Figure 9: Comparison between $\frac{SPM_{Counts}}{CSM_{Counts}}$ and AMM. The data is from the fluorescence of the Mn target operating with 100V of bias voltage.

Although this approach is not an exact measure of the condition in which the multiplicity equals 1, it does present a more strict rule in order to reduce the charge sharing effect, since it is well known that the CSM will present better behavior in reducing the effect. This is clearly shown in the threshold scan counts in SPM in Figure 3.

3.2.1 AMM curves

As the experiment has different energy calibration curves for SPM and CSM (Figures 5 and 6), in order to represent the threshold axis in energy values, there are different data points of energy thresholds for each operation mode. In order to compare and operate with this data, the CSM data points were converted to the energy threshold domain of the SPM data points via linear

interpolation. Each SPM data point was divided by the CSM data points interpolated to the SPM discrete energy domain in order to obtain $\frac{SPM_{Counts}}{CSM_{Counts}}$.

The obtained AMM curves for each target and bias voltage evaluated are presented in Figure 10. As expected the effect of the charge sharing is explicitly greater on lower energies, since the point at which $AMM = 1$ after the peak from the signal presence (the point of optimal threshold to be selected) is closer to the incident energy for Mn than Ni and Cu. For the Mn fluorescent photons, it is clearly not recommended to operate the bias voltage below 50V, since the optimal threshold via AMM is only reached after the signal. Also, the AMM can reach higher values for lower energies along the scan.

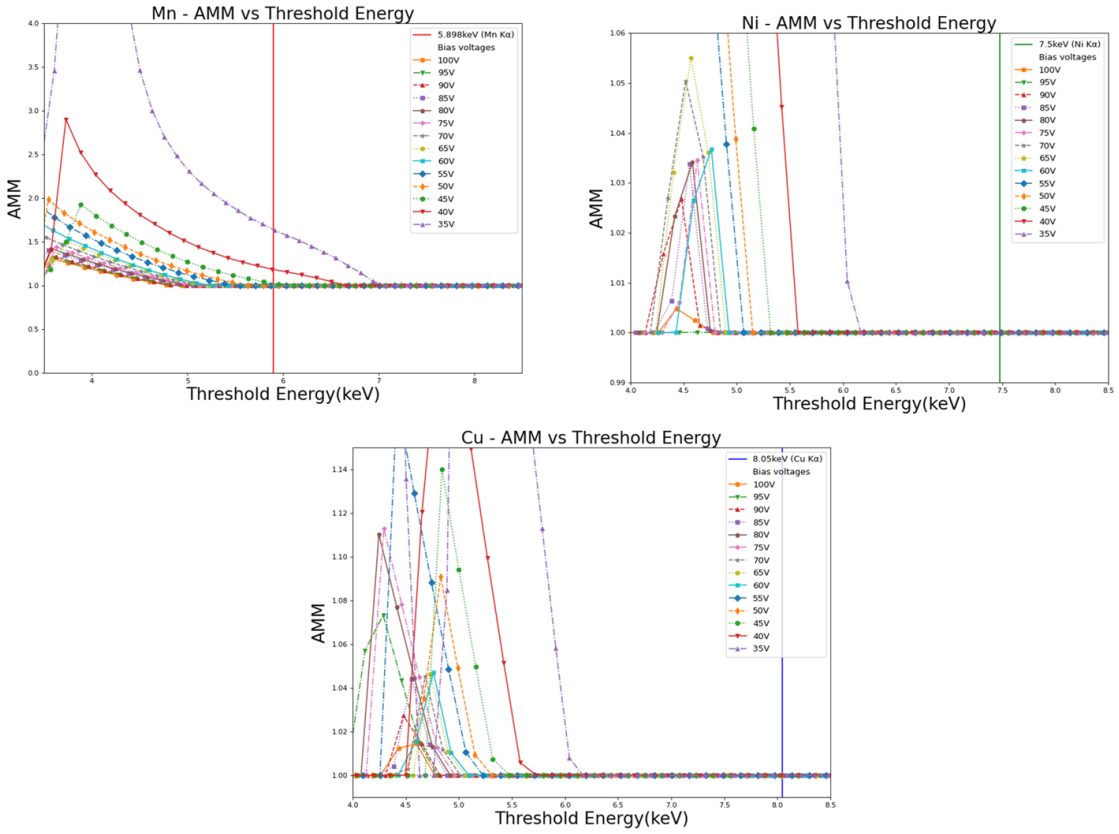

Figure 10: AMM curves for Mn, Ni and Cu fluorescent targets.

3.2.2 Optimal threshold via AMM

Based on the results shown in Figure 10 results, we can find the optimal threshold via AMM. In order to understand how the optimal threshold behaves along different incident energies, we can divide the optimal threshold by its incident energy as shown in Figure 11.

This optimal threshold value can be used even on different gain modes since it is only dependent on its incident energy and bias voltage, only being necessary for the calibration curve for the respective bias voltage and operation mode to convert the energy value to DAC steps. In summary, to operate using this optimal threshold in other gain modes it is not necessary to perform new AMM calculations, which experimentally need booth TS in SPM and CSM.

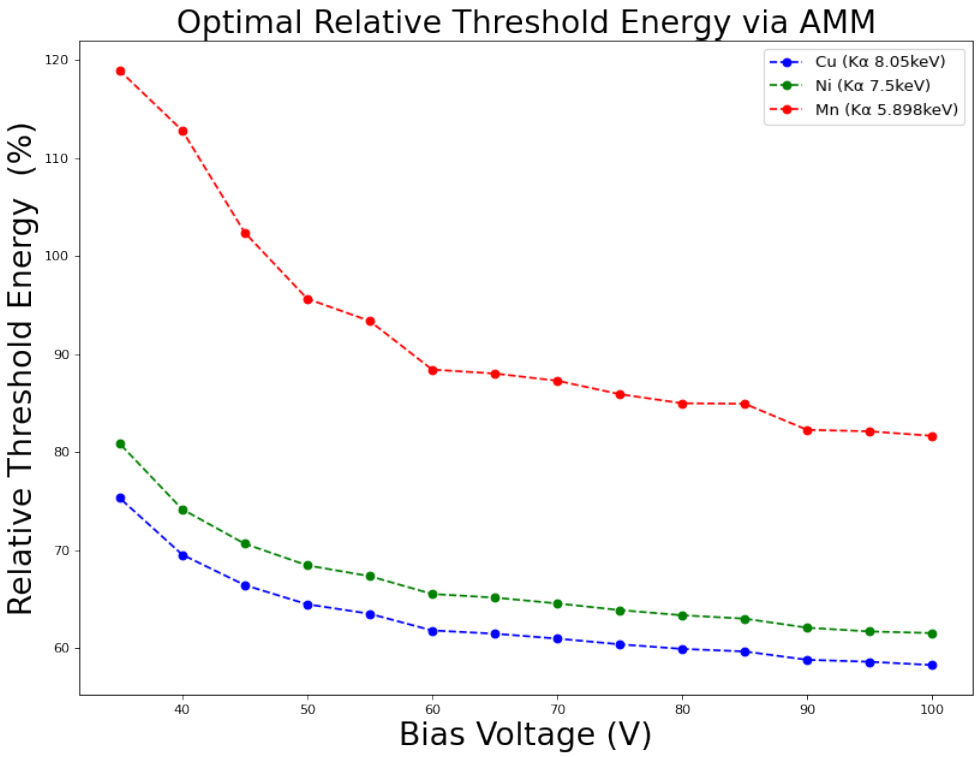

Figure 11: Optimal relative threshold via AMM for Mn, Ni and Cu fluorescent targets.

4. Conclusions and perspectives

The Approximated Mean Multiplicity was defined in order to have a practical way of evaluating the mean multiplicity. AMM can be used as a procedure to define an optimal threshold energy point to be used in acquisitions, while combining this optimal point with the SPM mode one can obtain less influence of the charge sharing effect while keeping optimal energy resolution. It's an alternative procedure to half of the incident energy threshold proposed in [4].

The calibration curve, establishing a linear relation between threshold level and threshold energy, was obtained for each operational condition of this study (bias voltage range of 35 to 100V, with step of 5V, for SPM and CSM, using the three available fluorescence targets for a total of 28 calibration curves). The incident energy peak position in the threshold level (while in digital steps) tends to appear early in the CSM mode, as the noise equalization causes a shift in the threshold level axis, the calibration corrects this deviation. The energy resolution is better in SPM mode and even better the higher the bias voltage is used for this mode of operation.

Future perspectives of this study are to compare threshold optimization procedures in relation to spatial resolution, and dual-energy experiments and investigate the assumption of $< m >= 1$ in CSM reproducing the multiplicity experiment from [8] for Medipix3RX.

References

[1] R. Campanelli, G. Gomes, M. Fernandes, L. Mendes, L. Rosa, R. Reis et al., *Large area hybrid detectors based on medipix3rx: commissioning and characterization at sirius beamlines*, *Journal of Instrumentation* **18** (2023) C02008.

[2] R. Ballabriga, J. Alozy, G. Blaj, M. Campbell, M. Fiederle, E. Frojdh et al., *The medipix3rx: a high resolution, zero dead-time pixel detector readout chip allowing spectroscopic imaging*, *Journal of Instrumentation* **8** (2013) C02016.

[3] H.C. Tolentino, M.M. Soares, C.A. Perez, F.C. Vicentin, D.B. Abdala, D. Galante et al., *Carnaúba: the coherent x-ray nanoprobe beamline for the brazilian synchrotron sirius/lnls*, in *Journal of Physics: Conference Series*, vol. 849, p. 012057, IOP Publishing, 2017.

[4] K. Mathieson, M. Passmore, P. Seller, M. Prydderch, V. O'Shea, R. Bates et al., *Charge sharing in silicon pixel detectors*, *Nuclear Instruments and Methods in Physics Research Section A: Accelerators, Spectrometers, Detectors and Associated Equipment* **487** (2002) 113.

[5] T. Koenig, E. Hamann, S. Procz, R. Ballabriga, A. Cecilia, M. Zuber et al., *Charge summing in spectroscopic x-ray detectors with high-z sensors*, *IEEE Transactions on Nuclear Science* **60** (2013) 4713.

[6] J. Rinkel, D. Magalhães, F. Wagner, E. Frojdh and R.B. Sune, *Equalization method for medipix3rx*, *Nuclear Instruments and Methods in Physics Research Section A: Accelerators, Spectrometers, Detectors and Associated Equipment* **801** (2015) 1.

[7] T. Michel, G. Anton, J. Durst, P. Bartl, M. Bohnel, M. Firsching et al., *Investigating the dqe of the medipix detector using the multiplicity concept*, in *2006 IEEE Nuclear Science Symposium Conference Record*, vol. 3, pp. 1955–1959, IEEE, 2006.

[8] T. Michel, G. Anton, M. Böhnel, J. Durst, M. Firsching, A. Korn et al., *A fundamental method to determine the signal-to-noise ratio (snr) and detective quantum efficiency (dqe) for a photon counting pixel detector*, *Nuclear Instruments and Methods in Physics Research Section A: Accelerators, Spectrometers, Detectors and Associated Equipment* **568** (2006) 799.